Inorganic Chemistry

pubs.acs.org/IC Article

High-Pressure-Stabilized Post-Spinel Phase of $CdFe_2O_4$ with Distinct Magnetism from Its Ambient-Pressure Spinel Phase

Beihong Li,[¶] Xubin Ye,[¶] Xiao Wang, Jie Zhang, Dabiao Lu, Haoting Zhao, Maocai Pi, Zhiwei Hu, Hong-Ji Lin, Chien-Te Chen, Zhao Pan,* Xiaomei Qin,* and Youwen Long*

Cite This: *Inorg. Chem.* 2023, 62, 9139−9145 Read Online

ACCESS | Metrics & More | Article Recommendations | Supporting Information

ABSTRACT: α-$CdFe_2O_4$ stabilizes its normal spinel structure due to the covalent Cd−O bond, in which all the connections between adjacent FeO_6 octahedral are edge-shared, forming a typical geometrically frustrated Fe^{3+} magnetic lattice. As the high-pressure methods were utilized, the post-spinel phase β-$CdFe_2O_4$ with a $CaFe_2O_4$-type structure was synthesized at 8 GPa and 1373 K. The new polymorph has an orthorhombic structure with the space group *Pnma* and an 11.5% higher density than that of its normal spinel polymorph (α-$CdFe_2O_4$) synthesized at ambient conditions. The edge-shared FeO_6 octahedra form zigzag S = 5/2 spin ladders along the *b*-axis dominating its low-dimensional magnetic properties at high temperatures and a long-range antiferromagnetic ordering with a high Néel temperature of T_{N1} = 350 K. Further, the rearrangement of magnetic ordering was found to occur around T_{N2} = 265 K, below which the competition of two phases or several couplings induce complex antiferromagnetic behaviors.

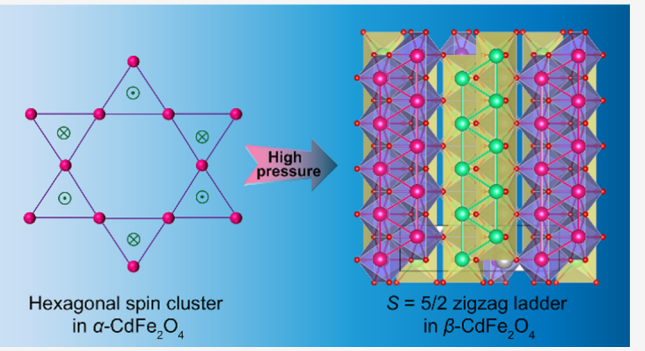

INTRODUCTION

Ternary spinel oxides (AB_2O_4) have been extensively investigated for their intriguing structural and physical properties,[1−5] as well as their wide variety of practical applications in electronic and magnetic devices[6] and several chemical reactions.[7,8] Spinel oxides usually crystallize into a cubic structure with the space group $Fd\bar{3}m$ (Figure 1a) and consist of a distorted face-centered close-packing oxygen lattice with cations occupying the tetrahedral and octahedral interstices, in which a single cation occupies the octahedral sites to form a normal spinel. In fact, the crystal structure is physically flexible, where electrostatic, elastic, and electronic boning energies must be considered to understand these oxides.[1] The ionic arrangement of the normal spinel leads to a three-dimensional framework through the common edge-sharing BO_6 octahedra, in which the sublattice of B cations is constructed by corner-sharing regular tetrahedrons (Figure 1b), therefore forming a typical completely geometrical frustration in magnetism.

High-pressure-induced structural transformation of spinel is a significant subject in both geoscience and materials science.[9−12] Such transition plays an important role in modeling the properties of Earth's transition zone and mantle, such as seismic interpretation, which induces large volume collapse, and changes in magnetic and electric interaction pathways, such as the formation of intriguing spin structures. Under high pressure, in general, the spinel oxide transforms into the so-called post-spinel phase,[13] which has also been discovered naturally in the Suizhou meteorite.[9,12] The framework of post-spinel is composed of the coexistence of common corner- and edge-sharing octahedra, and the ambient A site tetrahedral interstices are distorted into 8-fold-coordinated caves (Figure 1c−f). As a result, the post-spinel polymorph exhibits a more compact structure than its corresponding normal spinel counterpart. Meanwhile, magnetic frustrations of normal spinel are partially released, and novel spin structures and magnetic phenomena thus can be expected.[14,15]

$CaFe_2O_4$ has attracted special attention because of its orthorhombic *Pnma* post-spinel structure that does not require high-pressure treatment.[16,17] As proposed by Goodenough,[18] both cation−cation direct exchange within the ladders and cation−anion−cation indirect coupling between the adjacent ladders should be considered in this structure (as indicated by arrows and J labels in Figure 1). Two types of spin structures indicated by the A (↑↑↓↓) and B (↑↓↑↓) phases are proposed in $CaFe_2O_4$,[19,20] where the magnetic moments aligned parallel

Received: March 28, 2023
Published: May 31, 2023

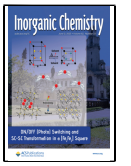

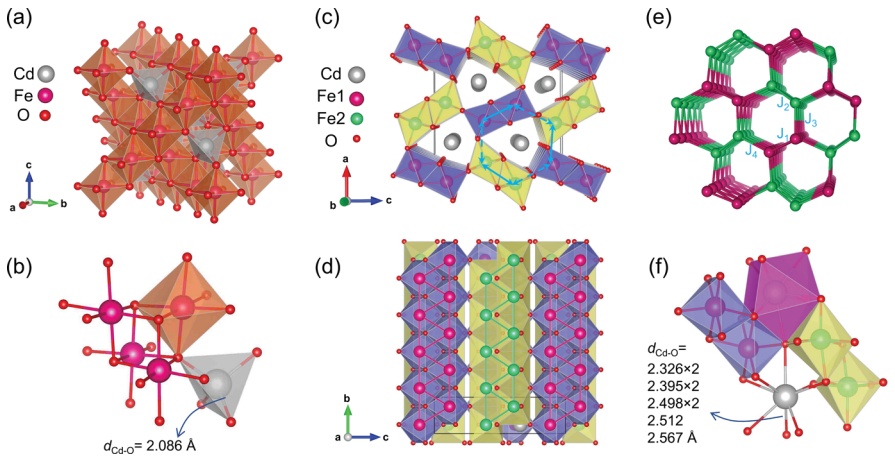

Figure 1. Crystal structures of two polymorphic $CdFe_2O_4$. (a) Schematic crystal structure and (b) local connections of FeO_6 octahedra and CdO_4 tetrahedron of α-$CdFe_2O_4$. (c) Crystal structure of β-$CdFe_2O_4$ projected along [010] and (d) [100], where zigzag ladders are clearly shown. (e) Fe atoms form hexagonal tunnels along the *b*-axis arranged in a distorted honeycomb lattice in β-$CdFe_2O_4$. (f) Local connections of FeO_6 octahedra and CdO_8 units of β-$CdFe_2O_4$.

to the *b*-axis forming ferromagnetic stripes. The competing phases can induce the formation of metastable antiphase boundaries and solitary magnons.[14,15,21,22] These results indicate that the ferromagnetic coupling within Fe ladders nearest to Fe−O−Fe with a bond angle of ∼90° is relatively strong, and the antiferromagnetic couplings through cation−cation direct and next-nearest to Fe−O−Fe with a bond angle of ∼100° via indirect pathways are comparable. Therefore, a slight change in bond length and angle may break the magnetic coupling balance in $CaFe_2O_4$ and induce novel magnetic structures and phenomena.

We note that Ca^{2+} and Cd^{2+} have similar ionic radii of 1.12 and 1.10 Å, respectively, but their ferrites present completely different crystal structures, the latter being normal spinel. This stems from the fact that the outer d shell of Cd^{2+} has a smaller energy gap with the 2p orbital of O^{2-} than noble gas-type Ca^{2+}, and it is easier to form covalent bonds and adapt to the tetrahedral coordination of A-site in the normal spinel.[1] Therefore, in spinel $CdFe_2O_4$, the application of external forces (i.e., high pressure) could increase structural distortion and destroy the covalent bond turning into an ionic bond, which may cause the spinel polymorph to collapse into a new structure, such as the post-spinel structure. In this paper, we successfully synthesized the post-spinel polymorph β-$CdFe_2O_4$ for the first time utilizing the high-pressure and high-temperature methods. Comprehensive investigations were performed to examine the crystal structure, charge state, and magnetic properties of both $CdFe_2O_4$ polymorphs. We found that β-$CdFe_2O_4$ crystallizes into the $CaFe_2O_4$-type orthorhombic structure (#62, *Pnma*) and is significantly denser than the ambient phase by 11.5%. The magnetic properties of α-$CdFe^{3+}{}_2O_4$ are dominated by hexagonal spin clusters, exhibiting short-range spin ordering over a wide range of temperatures. Intriguingly, the zigzag ladders and the honeycomb Fe^{3+} lattice determine the magnetic properties of β-$CdFe_2O_4$, which shows similar magnetic behaviors to $CaFe_2O_4$. However, the Néel temperature of β-$CdFe_2O_4$ reaches as high as 350 K, which is much higher than that of $CaFe_2O_4$ (180 K). In addition, a second magnetic transition occurs around 265 K, which was assigned to the transition from B (↑↓↑↓) to phase A (↑↑↓↓). At lower temperatures, some complex antiferromagnetic behaviors have also been observed owing to the competition between the two phases.

EXPERIMENTAL METHODS

Polycrystalline powders of α-$CdFe_2O_4$ were prepared under the conventional solid−state reaction. Highly pure (>99.9%) CdO and Fe_2O_3 powders were used as starting materials. They were thoroughly mixed with a 1:1 molar ratio using an agate mortar within an argon-filled glovebox and heated in a muffle furnace at 1173 K in the air for 24 h. Polycrystalline β-$CdFe_2O_4$ samples were synthesized via a high-pressure and high-temperature technique with the same starting materials. The mixtures were pressed into a gold capsule with a 3.0 mm diameter and a 4.0 mm height in the glovebox filled with argon. The capsule was put into an *h*-BN sleeve and then inserted into a cylindrical graphite heater, the end of which was contacted with Mo disks. A cube of pyrophyllite acted as the pressure medium. The sample was treated at 8 GPa and 1373 K for 30 min on a cubic-anvil-type high-pressure apparatus. At the end of heating, the sample was quenched to room temperature (RT), and the high pressure was released slowly for 6 h. The powder products were pressed into bulk under 6 GPa at RT, and bulk pieces for both phases were used for physical property measurements.

The phase identification and crystal structure analysis of powders were carried out by powder X-ray diffraction (XRD) at RT using a Huber diffractometer with Cu-$K_{\alpha 1}$ radiation (λ = 1.54056 Å) in the 2θ range of 10−100°. Rietveld analyses for XRD data were performed to refine the crystallographic parameters using the GSAS program.[23] The valence state of Fe was investigated by soft XAS at the Fe-$L_{2,3}$ edges, measured at the BL011A beamline in the National Synchrotron Radiation Research Center (NSRRC) using the total electron yield mode at RT. Magnetic susceptibility and magnetization were measured using a superconducting quantum interference device magnetometer (Quantum Design, MPMS-VSM). The magnetic susceptibility data were collected in zero-field-cooled (ZFC) and field-cooled (FC) modes at a magnetic field of 0.1 T. The isothermal magnetic hysteresis loops at different temperatures were measured between −5 T and +5 T. The magnetic data above 300 K were collected on a MicroSense vibrating sample magnetometer equipped on MPMS. Specific heat data and the frequency-dependent ac magnetization (χ') were obtained on a physical property measurement system (Quantum Design, PPMS-9T).

RESULTS AND DISCUSSION

Polycrystalline samples of spinel (α-) and post-spinel (β-) $CdFe_2O_4$ have been synthesized under ambient and high-

https://doi.org/10.1021/acs.inorgchem.3c01002
Inorg. Chem. 2023, 62, 9139−9145

pressure conditions, respectively. Figures 2 and S1 display the XRD patterns of both phases and corresponding structural

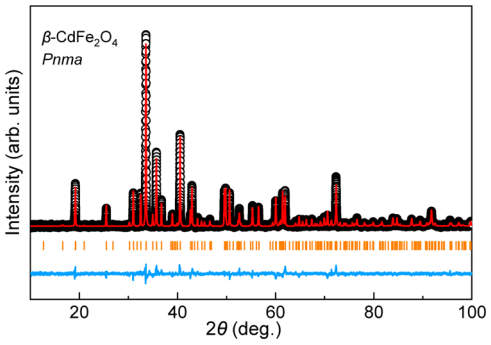

Figure 2. XRD pattern with Rietveld refinement results at RT for β-$CdFe_2O_4$. The observed (black circles), calculated (red line), and difference (blue line) profiles are shown. The orange ticks indicate the allowed Bragg reflections with the space group *Pnma*.

refinement results based on the Rietveld method. Tables S1 and S2 summarize the detailed lattice parameters, atom sites, bond lengths, and angles. α-$CdFe_2O_4$ crystallizes into a cubic normal spinel structure (Figure 1a,b) with the space group $Fd\bar{3}m$ and the lattice parameter a = 8.7041(8) Å, agreeing well with previous reports.[24] For the XRD pattern of high-pressure polymorph, detailed analysis demonstrates that the sample was free of any impurities, and all the diffraction peaks can be well indexed into an orthorhombic structure and further confirmed by the Rietveld refinement as the $CaFe_2O_4$-type structure with the space group *Pnma*. The lattice parameters were determined to be a = 9.2331(1) Å, b = 2.9935(2) Å, and c = 10.6753(2) Å. As shown in Figure 1c−f, in this definite structure, the Cd, Fe, and O atoms occupy one, two, and four, respectively, special Wyckoff positions 4c (x, 1/4, and z). The Fe ions at two different crystallographic sites, labeled Fe1 and Fe2, are both still octahedrally coordinated with the neighboring O ions. Symmetry equivalent FeO_6 octahedra with shared edges form double-rutile chains along the b-axis, while it is a corner shared connection between nonequivalent FeO_6 octahedra. Thus, in the ac plane, the alternating distribution of shared edges and shared corners forms a distorted honeycomb structure (Figure 1c,d), and the Cd ions are accommodated in hexagonal tunnels. Along the b-axis, within the chains, Fe ions construct a zigzag triangular ladder (Figure 1d), containing two types of Fe−Fe distances, the shorter one parallel to the b-axis and the longer one sloping to the bc plane.

Compared to the tetrahedrally coordinated CdO_4 in α-$CdFe_2O_4$, the 8-fold-coordinated CdO_8 is formed in β-$CdFe_2O_4$ (Figure 1b,f), where the Cd−O bond distance in α-$CdFe_2O_4$, 2.086 Å, is significantly smaller than that in β-$CdFe_2O_4$, 2.360−2.556 Å, which indicates that the former is a typical covalent bond, while the latter is ionic, corresponding to the overestimated valence +2.34 of Cd in α-$CdFe_2O_4$ calculated by the bond-valence sum (BVS) method (Table S2). However, the bond lengths in FeO_6 octahedra only change slightly between two polymorphs, and the Fe^{3+} valence states are estimated by the BVS method (Table S2).

As is well known, the soft XAS spectra at the 3d transition metal element $L_{2,3}$ edges are highly sensitive to their valence states[25−27] and local environment.[28,29] Thus, XAS spectroscopy for two $CdFe_2O_4$ polymorphs on Fe $L_{2,3}$ edges have been carried out, as shown in Figure 3. The spectra correspond to

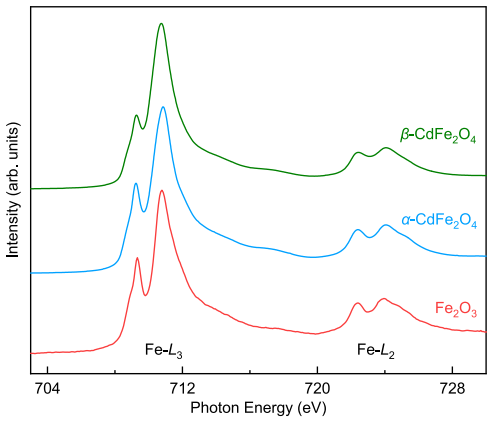

Figure 3. Fe-$L_{2,3}$ XAS spectra of α-$CdFe_2O_4$ and β-$CdFe_2O_4$ together with the related reference $Fe^{3+}{}_2O_3$ for comparison.

Fe 2p → Fe 3d transition and are dominated by multiplet effects, which are split into the Fe $2p_{3/2}$ (L_3) and $2p_{3/2}$ (L_2) regions. The lines of two polymorphs exhibit exactly similar spectral features in both peak energy positions and line shapes to those of the standard $Fe^{3+}{}_2O_3$ reference, unveiling the Fe^{3+} valence states in both phases of $CdFe_2O_4$. Both polymorphs of $CdFe_2O_4$ show Mott−Hubbard insulating behaviors with resistivities larger than 10^5 Ω·cm due to the strong electron−electron correlation, which is consistent with the common $Fe^{3+}O_6$ framework.[30]

Figure 4a shows the temperature-dependent magnetic susceptibility curves of α-$CdFe_2O_4$ measured in ZFC and FC modes at 0.1 T. The magnetic transition occurs at the critical temperature T_{dc} ~ 25 K. We note that the ZFC and FC curves show considerable separation and that the FC curve tends to be saturated[31] below T_{dc}, indicating the nature of the short range spin ordering. As can be seen from the inverse

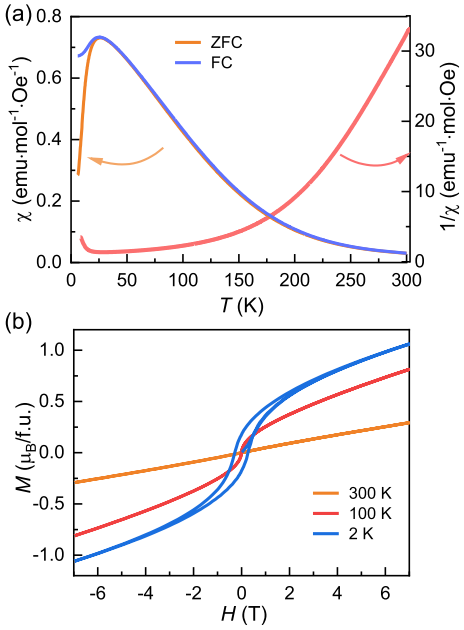

Figure 4. Magnetic properties of α-$CdFe_2O_4$. (a) Temperature-dependent magnetic susceptibility measured at 0.1 T. The pink curve shows the inverse susceptibility $\chi^{-1}(T)$. (b) Field-dependent isothermal magnetization loops measured at several selected temperatures.

https://doi.org/10.1021/acs.inorgchem.3c01002
Inorg. Chem. 2023, 62, 9139−9145

susceptibility plot, the measured data deviates from the linear relationship of Curie−Weiss law, and the measured temperature range seems too narrow to get reliable quantitative fitting parameters, which is consistent with the results of the single crystal.[26] Thus, magnetic couplings are active near RT despite the transition temperature as low as 25 K. Figure 4b presents the isothermal magnetization curves of α-$CdFe_2O_4$ measured at 2, 100, and 300 K. All curves are unsaturated as the field increases to 7 T, and magnetic hysteresis becomes more and more significant with decreasing temperature. These behaviors do not have regular mapping characteristics to the $M-T$ curve and account for the short-range magnetic coupling.[32,33] It should be noted that although the $M-H$ curve at 300 K is perfectly linear, its slope is considerable, again indicating that the magnetic interaction works at high temperatures.

The temperature-dependent specific heat and ac magnetization for α-$CdFe_2O_4$ (Figure S2) also demonstrate its short-range magnetic coupling behaviors around T_{dc}. The considerable magnetic contribution is clearly shown in the $C_m/T-T$ plot as shown in the inset of Figure S2a, but the magnetic entropy S_m (12.2 J·mol^{-1}·K^{-1}) obtained was much lower than the expected value of $2 \times R \ln 6 = 29.8$ J·mol^{-1}·K^{-1} for $CdFe_2O_4$. This could be explained by the gradual release of magnetic entropy at high temperatures, which echoes the short-range magnetic coupling observed on magnetic measurements at 300 K and the fact that the spin state still retains a large amount of entropy when it is as low as 2 K. The ac magnetization was measured at 10 Oe and different frequencies varying from 133 to 6333 Hz (Figure S2b), and the frequency dependence of T_f can be well described by the conventional dynamic slowing down model[34] (inset of Figure S2b). The fitting results (Table S3) confirm the spin cluster nature of α-$CdFe_2O_4$.

In the normal spinel, both $Fe^{3+}-Fe^{3+}$ Heisenberg direct and 90° $Fe^{3+}-O-Fe^{3+}$ indirect interactions coexist and could exhibit competition between antiferromagnetic and ferromagnetic interactions,[35] as observed in $ZnFe_2O_4$ and α-$CdFe_2O_4$ single crystals, respectively.[26,36] Tchernyshyov et al.[37] proposed that hexagonal spin clusters, constructed by six Fe^{3+} tetrahedra, dominate its magnetism. The inelastic neutron scattering study shows that the clusters exhibit a large correlation length and very gradual dissociation with increasing temperature.[26] In fact, the magnetism of α-$CdFe_2O_4$ is very sensitive to the slight changes in lattice constants or distances between Fe atoms and the size and shape of the synthesized particles under different conditions. For example, both long- and short-range spin ordering has been found in single crystals,[24,26] spin-glass states in thin films prepared via the sol−gel method,[38] and even ferromagnetic behavior with Curie temperature up to 553 K in the ultrafine particles.[39] Thus, in our synthesized α-$CdFe_2O_4$, big hexagonal spin clusters account for its short-range couplings and spin dynamics at low temperatures.

The magnetic properties of β-$CdFe_2O_4$ were investigated in a wider temperature range of 2−800 K, as shown in Figure 5. The temperature dependence of the ZFC and FC magnetic susceptibility curves of β-$CdFe_2O_4$ below 380 K was measured at 0.1 T. Above 380 K, the ZFC magnetic susceptibility data were collected at 0.1 T. Even though the temperature has reached 800 K, it still seems too narrow to accurately fit the parameters of the paramagnetic region. At high temperatures, the magnetic susceptibility changes slowly with cooling and shows a broadened maximum centered at about T_{N1} = 350 K,

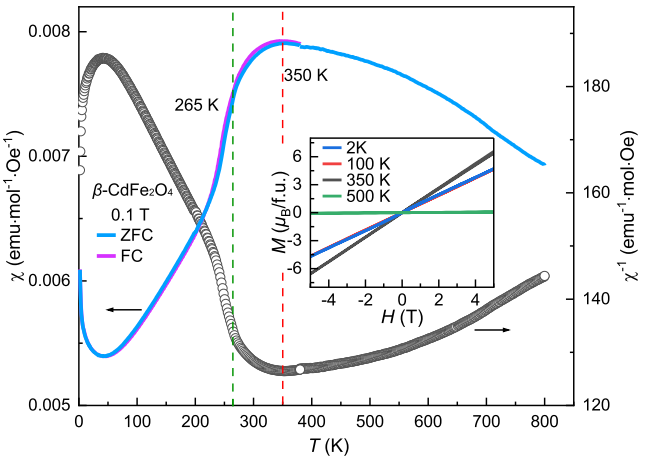

Figure 5. Magnetic properties of β-$CdFe_2O_4$. Temperature-dependent magnetic susceptibility was measured at 0.1 T. The inset shows field-dependent isothermal magnetization loops measured at selected temperatures.

much higher than that of the isostructural $CaFe_2O_4$ (180 K),[40] indicating low-dimensional spin structures like the isostructural β-$CdCr_2O_4$.[11] With further cooling, the susceptibility drops rapidly and shows an inflection point at 240 K. Until 40 K, a minimum appears, below which it abruptly rises monotonically. The inset of Figure 5 displays field-dependent isothermal magnetization loops measured at several critical temperatures. At 500 K, the linear behavior of the $M-H$ curve with a delicate slope corresponds to its paramagnetic state. When cooled to 350 K, the linear behavior is preserved, but the slope and magnetization values increase substantially, indicating the formation of the antiferromagnetic spin ordering. Interestingly, at 100 K, the $M-H$ curve lies between the curves of 350 and 500 K, suggesting that it constructs another long-range spin state, and the linear behavior confirms that it is antiferromagnetic. The lines of 2 and 100 K coincide completely, indicating that there is a consistent magnetic ordering state in this temperature region, and the anomaly around 40 K on the $M-T$ curve is caused by some complex or noncollinear antiferromagnetic competitions, which is also consistent with isostructural β-$CdCr_2O_4$.[11]

Figure 6 shows the temperature-dependent specific heat C_p for β-$CdFe_2O_4$ in the temperature range of 2−300 K. A sharp λ-type specific heat anomaly is observed around T_{N2} = 265 K, which first confirms the long-range antiferromagnetic ordering, and second, T_{N2} is much lower than T_{N1} = 350 K observed on magnetization curves, indicating that this transition may be responsible for the rearrangement of two long-range spin structures. For further quantitative analysis, we use the Debye−Einstein model fitting to describe the lattice-specific heat by the equation[41] $C_p = a\frac{9R}{x_D^3}\int_0^{x_D}\frac{x^4e^x}{(e^x-1)^2}dx + b\,3R\frac{x_E^2e^xE}{(e^xE-1)^2}$, where R is the universal gas constant, a and b are the number of vibrating modes per f.u., $x_D = T_D/T$, $x_E = T_E/T$, and T_D and T_E are the Debye and Einstein temperatures, respectively. The fitting result was plotted as a red line in Figure 6a and yields a = 3.1, b = 4.7, T_D = 299 K, and T_E = 579 K. Thus, the magnetic specific heat C_m was obtained by subtracting $C_{lattice}$ from the observed C_p. Further, by integrating C_m/T over the observed temperature range, the magnetic entropy S_m was obtained as shown in Figure 6b. S_m is saturated to 2.1 J·mol^{-1}·K^{-1}, which is an order of magnitude lower than the expected value of 29.8 J·

https://doi.org/10.1021/acs.inorgchem.3c01002
Inorg. Chem. 2023, 62, 9139−9145

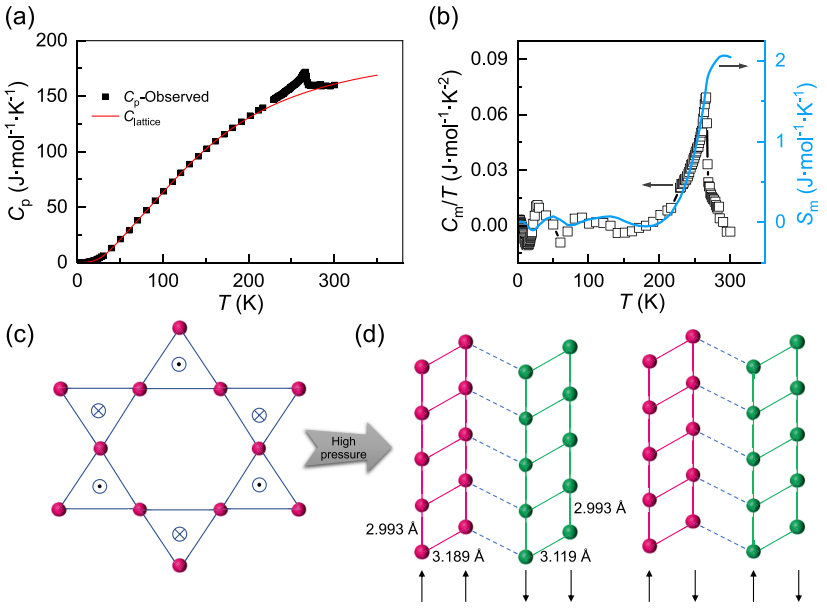

Figure 6. (a) Temperature dependence of specific heat for β-$CdFe_2O_4$ below 300 K under zero field. The solid line represents the lattice contribution $C_{lattice}$ estimated by the Debye−Einstein model. (b) Magnetic contribution to specific heat (left), plotted as $C_m/T \sim T$, obtained by subtracting $C_{lattice}$ from the observed total C_p. The magnetic entropy S_m (right) was evaluated by integrating C_m/T over the observed temperature range. (c) Illustration of the hexagonal spin clusters in α-$CdFe_2O_4$, where ⊙ and ⊗ denote that the fourth corner of the tetrahedron is oriented up or down, respectively. (d) Schematic view of A (↑↑↓↓)- and B (↑↓↑↓)-type magnetic structures in β-$CdFe_2O_4$.

mol^{-1}·K^{-1} for the formation of a magnetically ordered phase transition from the paramagnetic state. Therefore, a large proportion of the magnetic entropy is released at higher temperatures, corresponding to the magnetic phase transition around 350 K.

High pressure forces the destruction of the covalent bond of Cd−O and changes the coordination environment of Cd−O, which further changes the connections of FeO_6 octahedra. In this transformation, part of the edge-shared connection is transformed into a corner-shared connection. Accordingly, the magnetic interaction path has changed substantially. In α-$CdFe_2O_4$, six corner-shared Fe tetrahedra form big hexagonal spin clusters by alternating up and down orientations, as shown in Figure 6c, in which all Fe^{3+}−Fe^{3+} couplings are equivalent and completely geometrically frustrated. As a result, the macroscopic magnetism of α-$CdFe_2O_4$ exhibits short-range ordering dominated by hexagonal spin clusters, and it works at relatively high temperatures due to its large correlation length. Because β-$CdFe_2O_4$ shows very similar magnetic behaviors to isostructural $CaFe_2O_4$, we believe that they should have the same magnetic structure. As shown in Figure 6c,d, zigzag ladders dominate its anisotropic antiferromagnetic orderings in β-$CdFe_2O_4$. At high temperatures, the B (↑↓↑↓) phase is first established, and with cooling, the A (↑↑↓↓) phase is gradually derived, and an antiphase boundary along the c-axis is formed between the two phases. At lower temperatures, both phases coexist, and their competitions lead to complex magnetic behaviors.[14,15,19,21,22] In Goodenough's model,[18] the cation−cation interactions (antiferromagnetic) within zigzag ladders and the 180° indirect cation−anion−cation interaction (antiferromagnetic) between corner-shared ladders may be significant. Thus, geometrical frustrations are established in the triangular or honeycomb lattice (see Figure 1d,e). However, both t_{2g} and e_g orbitals on Fe^{3+} are half-filled, enhancing the 90° indirect coupling (ferromagnetic) via the $p\sigma$, $p\sigma'$ pathway. In addition, the two-type Fe−Fe distances that built up the ladders are not equivalent. The shorter one parallel to the ladder eventually exhibits a sum ferromagnetic coupling, forming robust ferromagnetic stripes along the b-axis, while the longer cation−cation and indirect couplings are comparable and compete with cooling, inducing the transition between the B (↑↓↑↓) and A (↑↑↓↓) phases.

CONCLUSIONS

In summary, we prepared polycrystalline ferrite α-$CdFe_2O_4$ with a normal spinel structure under ambient conditions, while its post-spinel polymorph β-$CdFe_2O_4$ was successfully synthesized for the first time under high-pressure and high-temperature conditions. Distinct physical properties were observed in these two types of $CdFe_2O_4$ with different crystal structures. α-$CdFe_2O_4$ is completely geometrically frustrated, in which hexagonal spin clusters dominate its magnetic properties and exhibit short-range spin ordering over the observed temperature range, while for β-$CdFe_2O_4$, zigzag spin $S = 5/2$ ladders and the honeycomb Fe^{3+} lattice determine the magnetic properties, which experience low-dimensional magnetic behaviors, and form a long-range antiferromagnetic ordering of B (↑↓↑↓) phase at T_{N1} = 350 K. In addition, a sharp anomaly in specific heat appears around T_{N2} = 265 K, indicating the rearrangement of spin ordering. At lower temperatures, A (↑↑↓↓) and B (↑↓↑↓) phases coexist, and their competition leads to some complex antiferromagnetic behaviors. The present study suggested that the competition of multiple direct and indirect interactions, subtly regulated by the distribution of bond lengths and angles, leads to the difference of antiferromagnetic ordering temperature between β-$CdFe_2O_4$ and $CaFe_2O_4$, as well as their rich magnetic properties.

https://doi.org/10.1021/acs.inorgchem.3c01002
Inorg. Chem. 2023, 62, 9139−9145

■ ASSOCIATED CONTENT

Supporting Information

The Supporting Information is available free of charge at https://pubs.acs.org/doi/10.1021/acs.inorgchem.3c01002.

Details of the Rietveld refinements, specific heat, and structural parameters of α-$CdFe_2O_4$ and β-$CdFe_2O_4$ (PDF)

Accession Codes

CCDC 2252228 contains the supplementary crystallographic data for this paper. These data can be obtained free of charge via www.ccdc.cam.ac.uk/data_request/cif, or by emailing data_request@ccdc.cam.ac.uk, or by contacting The Cambridge Crystallographic Data Centre, 12 Union Road, Cambridge CB2 1EZ, UK; fax: +44 1223 336033.

■ AUTHOR INFORMATION

Corresponding Authors

Zhao Pan − *Beijing National Laboratory for Condensed Matter Physics, Institute of Physics, Chinese Academy of Sciences, Beijing 100190, China;* orcid.org/0000-0002-8693-2508; Email: zhaopan@iphy.ac.cn

Xiaomei Qin − *Department of Physics, Shanghai Normal University, Shanghai 200234, China*; Email: xmqin@shnu.edu.cn

Youwen Long − *Beijing National Laboratory for Condensed Matter Physics, Institute of Physics, Chinese Academy of Sciences, Beijing 100190, China; University of Chinese Academy of Sciences, Beijing 100049, China; Songshan Lake Materials Laboratory, Dongguan, Guangdong 523808, China;* orcid.org/0000-0002-8587-7818; Email: ywlong@iphy.ac.cn

Authors

Beihong Li − *Department of Physics, Shanghai Normal University, Shanghai 200234, China; Beijing National Laboratory for Condensed Matter Physics, Institute of Physics, Chinese Academy of Sciences, Beijing 100190, China*

Xubin Ye − *Beijing National Laboratory for Condensed Matter Physics, Institute of Physics, Chinese Academy of Sciences, Beijing 100190, China;* orcid.org/0000-0002-5739-8318

Xiao Wang − *Beijing National Laboratory for Condensed Matter Physics, Institute of Physics, Chinese Academy of Sciences, Beijing 100190, China;* orcid.org/0000-0001-8139-4192

Jie Zhang − *Beijing National Laboratory for Condensed Matter Physics, Institute of Physics, Chinese Academy of Sciences, Beijing 100190, China; University of Chinese Academy of Sciences, Beijing 100049, China*

Dabiao Lu − *Beijing National Laboratory for Condensed Matter Physics, Institute of Physics, Chinese Academy of Sciences, Beijing 100190, China; University of Chinese Academy of Sciences, Beijing 100049, China*

Haoting Zhao − *Beijing National Laboratory for Condensed Matter Physics, Institute of Physics, Chinese Academy of Sciences, Beijing 100190, China; University of Chinese Academy of Sciences, Beijing 100049, China*

Maocai Pi − *Beijing National Laboratory for Condensed Matter Physics, Institute of Physics, Chinese Academy of Sciences, Beijing 100190, China; University of Chinese Academy of Sciences, Beijing 100049, China*

Zhiwei Hu − *Max Planck Institute for Chemical Physics of Solids, Dresden 01187, Germany;* orcid.org/0000-0003-0324-2227

Hong-Ji Lin − *National Synchrotron Radiation Research Center, Hsinchu 30076, Taiwan*

Chien-Te Chen − *National Synchrotron Radiation Research Center, Hsinchu 30076, Taiwan*

Complete contact information is available at: https://pubs.acs.org/10.1021/acs.inorgchem.3c01002

Author Contributions

[¶]B.L. and X.Y. contributed equally to this work.

Notes

The authors declare no competing financial interest.

■ ACKNOWLEDGMENTS

This work was supported by the National Natural Science Foundation of China (grant nos. 11934017, 12261131499, 11921004, and 22271309), the Beijing Natural Science Foundation (grant no. Z200007), the National Key R&D Program of China (grant no. 2021YFA1400300 and 2018YFA0305700), and the Chinese Academy of Sciences (grant no. XDB33000000). The research in Dresden was partially supported by the DFG through SFB 1143. The authors acknowledge the support from the Max Planck-POSTECH-Hsinchu Center for Complex Phase Materials.

■ REFERENCES

(1) Goodenough, J. B.; Loeb, A. L. Theory of Ionic Ordering, Crystal Distortion, and Magnetic Exchange Due to Covalent Forces in Spinels. *Phys. Rev.* **1955**, *98*, 391−408.

(2) Sickafus, K. E.; Wills, J. M.; Grimes, N. W. Structure of Spinel. *J. Am. Ceram. Soc.* **2004**, *82*, 3279−3292.

(3) Greedan, J. E. Geometrically frustrated magnetic materials. *J. Mater. Chem.* **2001**, *11*, 37−53.

(4) Jin, K.; He, G.; Zhang, X.; Maruyama, S.; Yasui, S.; Suchoski, R.; Shin, J.; Jiang, Y.; Yu, H. S.; Yuan, J.; Shan, L.; Kusmartsev, F. V.; Greene, R. L.; Takeuchi, I. Anomalous magnetoresistance in the spinel superconductor $LiTi_2O_4$. *Nat. Commun.* **2015**, *6*, 7183.

(5) Blanco-Gutiérrez, V.; Urones-Garrote, E.; Torralvo-Fernández, M. J.; Sáez-Puche, R. $ZnFe_2O_4$ Nanoparticles: Different Magnetic Behavior When They Are Hosted in Porous Structures. *Chem. Mater.* **2010**, *22*, 6130−6137.

(6) Grimes, N. W. The spinels: versatile materials. *Phys. Technol.* **1975**, *6*, 22−27.

(7) Yuan, C.; Wu, H. B.; Xie, Y.; Lou, X. W. Mixed transition-metal oxides: design, synthesis, and energy-related applications. *Angew. Chem., Int. Ed.* **2014**, *53*, 1488−1504.

(8) Ida, S.; Yamada, K.; Matsunaga, T.; Hagiwara, H.; Matsumoto, Y.; Ishihara, T. Preparation of p-Type $CaFe_2O_4$ Photocathodes for Producing Hydrogen From Water. *J. Am. Chem. Soc.* **2010**, *132*, 17343−17345.

(9) Chen, M.; Shu, J.; Mao, H. K.; Xie, X.; Hemley, R. J. Natural occurrence and synthesis of two new postspinel polymorphs of chromite. *Proc. Natl. Acad. Sci. U.S.A.* **2003**, *100*, 14651−14654.

(10) Irifune, T.; Fujino, K.; Ohtani, E. A new high-pressure form of $MgAl_2O_4$. *Nature* **1991**, *349*, 409−411.

(11) Arevalo-Lopez, A. M.; Dos santos-Garcia, A. J.; Castillo-Martinez, E.; Duran, A.; Alario-Franco, M. A. Spinel to $CaFe_2O_4$ transformation: mechanism and properties of β-$CdCr_2O_4$. *Inorg. Chem.* **2010**, *49*, 2827−2833.

(12) Chen, M.; Shu, J.; Xie, X.; Mao, H. K. Natural $CaTi_2O_4$-structured $FeCr_2O_4$ polymorph in the Suizhou meteorite and its significance in mantle mineralogy. *Geochim. Cosmochim. Acta* **2003**, *67*, 3937−3942.

(13) Ling, C.; Mizuno, F. Phase Stability of Post-spinel Compound AMn_2O_4 (A = Li, Na, or Mg) and Its Application as a Rechargeable Battery Cathode. *Chem. Mater.* **2013**, *25*, 3062−3071.
(14) Stock, C.; Rodriguez, E. E.; Lee, N.; Green, M. A.; Demmel, F.; Ewings, R. A.; Fouquet, P.; Laver, M.; Niedermayer, C.; Su, Y.; Nemkovski, K.; Rodriguez-Rivera, J. A.; Cheong, S. W. Solitary Magnons in the S = 5/2 Antiferromagnet $CaFe_2O_4$. *Phys. Rev. Lett.* **2016**, *117*, 017201.
(15) Stock, C.; Rodriguez, E. E.; Lee, N.; Demmel, F.; Fouquet, P.; Laver, M.; Niedermayer, C.; Su, Y.; Nemkovski, K.; Green, M. A.; Rodriguez-Rivera, J. A.; Kim, J. W.; Zhang, L.; Cheong, S. W. Orphan Spins in the S = 5/2 Antiferromagnet $CaFe_2O_4$. *Phys. Rev. Lett.* **2017**, *119*, 257204.
(16) Das, R.; Karna, S.; Lai, Y.-C.; Chou, F.-C. Self-Adjusted Traveling Solvent Floating Zone Growth of Single Crystal $CaFe_2O_4$. Cryst. *Growth Des* **2015**, *16*, 499−503.
(17) Yamanaka, T.; Uchida, A.; Nakamoto, Y. Structural transition of post-spinel phases $CaMn_2O_4$, $CaFe_2O_4$, and $CaTi_2O_4$ under high pressures up to 80 GPa. *Am. Mineral.* **2008**, *93*, 1874−1881.
(18) Goodenough, J. B. Direct Cation- -Cation Interactions in Several Oxides. *Phys. Rev.* **1960**, *117*, 1442−1451.
(19) Watanabe, H.; Yamauchi, H.; Ohashi, M.; Sugimoto, M.; Okada, T.; Fukase, M. Neutron diffraction study of $CaFe_2O_4$. *J. Phys. Soc. Jpn.* **1967**, *22*, 939.
(20) Corliss, L. M.; Hastings, J. M.; Kunnmann, W. Magnetic Phase Equilibrium in Chromium-Substituted Calcium Ferrite. *Phys. Rev.* **1967**, *160*, 408−413.
(21) Lane, H.; Rodriguez, E. E.; Walker, H. C.; Niedermayer, C.; Stuhr, U.; Bewley, R. I.; Voneshen, D. J.; Green, M. A.; Rodriguez-Rivera, J. A.; Fouquet, P.; Cheong, S. W.; Attfield, J. P.; Ewings, R. A.; Stock, C. Metastable antiphase boundary ordering in $CaFe_2O_4$. *Phys. Rev. B* **2021**, *104*, 104404.
(22) Lane, H.; Stock, C.; Cheong, S. W.; Demmel, F.; Ewings, R. A.; Krüger, F. Nonlinear soliton confinement in weakly coupled antiferromagnetic spin chains. *Phys. Rev. B* **2020**, *102*, 024437.
(23) Larson, A.; Von Dreele, R. *General structure analysis system (GSAS)*, Los Alamos National Laboratory, 1994, Report No. Laur, 86, 748.
(24) Ostorero, J.; Mauger, A.; Guillot, M.; Derory, A.; Escorne, M.; Marchand, A. Influence of topological frustration on the magnetic properties of the normal oxyspinel $CdFe_2O_4$. *Phys. Rev. B* **1989**, *40*, 391−395.
(25) Tjeng, L. H.; Chen, C. T.; Cheong, S. W. Comparative soft-x-ray resonant-photoemission study on $Bi_2Sr_2CaCu_2O_8$, CuO, and Cu_2O. *Phys. Rev. B* **1992**, *45*, 8205−8208.
(26) Kamazawa, K.; Park, S.; Lee, S. H.; Sato, T. J.; Tsunoda, Y. Dissociation of spin objects in geometrically frustrated $CdFe_2O_4$. *Phys. Rev. B* **2004**, *70*, 024418.
(27) Mitra, C.; Hu, Z.; Raychaudhuri, P.; Wirth, S.; Csiszar, S. I.; Hsieh, H. H.; Lin, H. J.; Chen, C. T.; Tjeng, L. H. Direct observation of electron doping in $La_{0.7}Ce_{0.3}MnO_3$ using x-ray absorption spectroscopy. *Phys. Rev. B* **2003**, *67*, 092404.
(28) Burnus, T.; Hu, Z.; Wu, H.; Cezar, J. C.; Niitaka, S.; Takagi, H.; Chang, C. F.; Brookes, N. B.; Lin, H. J.; Jang, L. Y.; Tanaka, A.; Liang, K. S.; Chen, C. T.; Tjeng, L. H. X-ray absorption and x-ray magnetic dichroism study on Ca_3CoRhO_6 and Ca_3FeRhO_6. *Phys. Rev. B* **2008**, *77*, 205111.
(29) Hollmann, N.; Hu, Z.; Valldor, M.; Maignan, A.; Tanaka, A.; Hsieh, H. H.; Lin, H. J.; Chen, C. T.; Tjeng, L. H. Electronic and magnetic properties of the kagome systems $YBaCo_4O_7$ and $YBaCo_3MO_7$ (M = Al, Fe). *Phys. Rev. B* **2009**, *80*, 085111.
(30) Ye, X.; Zhao, J.; Das, H.; Sheptyakov, D.; Yang, J.; Sakai, Y.; Hojo, H.; Liu, Z.; Zhou, L.; Cao, L.; Nishikubo, T.; Wakazaki, S.; Dong, C.; Wang, X.; Hu, Z.; Lin, H. J.; Chen, C. T.; Sahle, C.; Efiminko, A.; Cao, H.; Calder, S.; Mibu, K.; Kenzelmann, M.; Tjeng, L. H.; Yu, R.; Azuma, M.; Jin, C.; Long, Y. Observation of novel charge ordering and spin reorientation in perovskite oxide $PbFeO_3$. *Nat. Commun.* **2021**, *12*, 1917.
(31) Edwards, S. F.; Anderson, P. W. Theory of spin glasses. *J. Phys. F: Met. Phys.* **1975**, *5*, 965−974.
(32) Mydosh, J. A. *Spin Glasses: An Experimental Introduction*; Taylor & Francis, 1993.
(33) Ye, X.; Liu, Z.; Wang, W.; Hu, Z.; Lin, H. J.; Weng, S. C.; Chen, C. T.; Yu, R.; Tjeng, L. H.; Long, Y. High-pressure synthesis and spin glass behavior of a Mn/Ir disordered quadruple perovskite $CaCu_3Mn_2Ir_2O_{12}$. *J. Phys.: Condens. Matter* **2020**, *32*, 075701.
(34) Pakhira, S.; Mazumdar, C.; Ranganathan, R.; Giri, S.; Avdeev, M. Large magnetic cooling power involving frustrated antiferromagnetic spin-glass state in R_2NiSi_3 (R = Gd, Er). *Phys. Rev. B* **2016**, *94*, 104414.
(35) Goodenough, J. B. *Magnetism and the Chemical Bond*; Interscience publishers, 1963.
(36) Kamazawa, K.; Tsunoda, Y.; Kadowaki, H.; Kohn, K. Magnetic neutron scattering measurements on a single crystal of frustrated $ZnFe_2O_4$. *Phys. Rev. B* **2003**, *68*, 024412.
(37) Tchernyshyov, O.; Moessner, R.; Sondhi, S. L. Order by distortion and string modes in pyrochlore antiferromagnets. *Phys. Rev. Lett.* **2002**, *88*, 067203.
(38) Reitz, C.; Suchomski, C.; Chakravadhanula, V. S.; Djerdj, I.; Jaglicic, Z.; Brezesinski, T. Morphology, microstructure, and magnetic properties of ordered large-pore mesoporous cadmium ferrite thin film spin glasses. *Inorg. Chem.* **2013**, *52*, 3744−3754.
(39) Yokoyama, M.; Sato, T.; Ohta, E.; Sato, T. Magnetization of cadmium ferrite prepared by coprecipitation. *J. Appl. Phys.* **1996**, *80*, 1015−1019.
(40) Das, R.; Karna, S.; Lai, Y. C.; Chou, F. C.; Chou, F. C. Self-Adjusted Traveling Solvent Floating Zone Growth of Single Crystal $CaFe_2O_4$. *Cryst. Growth Des.* **2016**, *16*, 499−503.
(41) Kittel, C. *Introduction to Solid State Physics*, 8; John Wiley & Sons, Inc., 2004.

https://doi.org/10.1021/acs.inorgchem.3c01002
Inorg. Chem. 2023, 62, 9139−9145